ELSEVIER

Contents lists available at ScienceDirect

# **Materials Letters**

journal homepage: www.elsevier.com/locate/matlet



# A novel cytocompatible, hierarchical porous Ti6Al4V scaffold with immobilized silver nanoparticles



Zhaojun Jia <sup>a</sup>, Ming Li <sup>a</sup>, Peng Xiu <sup>b</sup>, Xuchen Xu <sup>a</sup>, Yan Cheng <sup>a,\*</sup>, Yufeng Zheng <sup>a,c</sup>, Tingfei Xi <sup>a</sup>, Shicheng Wei <sup>a,d</sup>, Zhongjun Liu <sup>b</sup>

- a Center for Biomedical Materials and Tissue Engineering, Academy for Advanced Interdisciplinary Studies, Peking University, Beijing 100871, China
- <sup>b</sup> Department of Orthopedics, Peking University Third Hospital, Beijing 100191, China
- <sup>c</sup> Department of Advanced Materials and Nanotechnology, College of Engineering, Peking University, Beijing 100871, China
- d Department of Oral and Maxillofacial Surgery, School and Hospital of Stomatology, Peking University, Beijing 100871, China

## ARTICLE INFO

Article history: Received 8 July 2014 Received in revised form 3 May 2015 Accepted 16 May 2015 Available online 27 May 2015

Keywords: Electron beam melting (EBM) Micro-arc oxidization (MAO) Poly(dopamine) (PD) Silver nanoparticles (AgNPs)

## ABSTRACT

Owing to their mechanical properties and bioinertness titanium alloys remain the preferred load-bearing implant material in orthopedics. However, unsatisfactory osteointegration and risks of infection are the two major problems. Herein, Ti6Al4V prostheses with 3D hierarchical (macro/micro-nano) porosity were constructed by combining the state-of-art electron beam melting (EBM) additive manufacturing (AM) process with a traditional micro-arc oxidization (MAO) technique for enhanced integration with bone tissues, and as a measure to improve their antimicrobial properties, releasable silver nanoparticles (AgNPs) were homogeneously immobilized on the multi-scaled porous surfaces via a mussel-inspired strategy. The cytocompatibility of the engineered scaffolds (EBM–MAO/Ag) outperformed the untreated, due to synergistic benefits from micro/nano-porous topography and adhesive chemical composition.

#### 1. Introduction

Mechanical properties and biological inertness endow titanium-based implants with advantages in orthopedic applications including bone substitution and total joint replacement surgeries [1]. However, biomechanical mismatch associated with their excessively high elastic modulus unfortunately leads to stress shielding effect and therefore aseptic loosening, osteopenia, and eventually revision surgery [1, 2]. With tunable mechanical properties, porous titanium has emerged as a promising solution, and their optimized cellular structures are supposed to provide an extended framework for osteointegration. EBM is one of the most appealing AM techniques that allow us to flexibly manufacture porous architectures with customized shapes, interconnected porosity and appropriate mechanical strength at an economical cost [3]. Whereas, the pore walls (topology, roughness) are far from satisfactory, e.g. large surface roughness and loose powder particles [4], rendering biocompatible surface modification a necessity. MAO is a convenient and frequently performed technique to fabricate micro-nano porous coatings in situ that bind well to substrate. More importantly, the resultant oxide coatings (usually TiO<sub>2</sub>) show excellent biocompatibility [5], bioactivity [6], osseointegration capability [7], and potential to inhibit toxic ion release (e.g.  $Al^{3+}$  and  $V^{n+}$ ). Moreover, it is suitable for implants with sophisticated shapes and curved surfaces, such as additive manufactured prostheses. Consequently, hierarchical macro/micro-nano structure/topography for titanium implants could be easily established by a combined EBM–MAO strategy. Still, biomaterial-associated infections (BAI) occasionally cause implant failures whose incidence in orthopedics is always standing between 2% and 5% [8]. AgNPs act as a highly-efficient and broadspectrum antimicrobial agent that simultaneously repel and kill bacteria via direct surface contact and/or lasting release of  $Ag^+$  [9]. Further, it could reduce the development of drug-resistant mutation [10]. Given its potential cytotoxicity [11], the challenge is to develop nano-silver engineered orthopedic implants without hindering cell functions or sacrificing osteogenesis.

In this work, we aimed to demonstrate a 3D hierarchical porous Ti6Al4V construct with osseointegrative potential by EBM–MAO. To improve its antimicrobial activity, the powerful mussel-inspired poly(dopamine) (PD) route was chosen to deposit AgNPs onto the micro-roughened surface due to its facility, adhesive property and excellent biocompatibility, and the fact that it anchors onto virtually any type and shape of surfaces as well [12]. The structure/morphology and chemical composition of the resultant nano-silver immobilized EBM–MAO scaffolds were investigated, and their cytocompatibility with osteoblast-like MG63 cells were evaluated in vitro.

<sup>\*</sup> Corresponding author. Fax: +86 10 62753404. E-mail address: chengyan@pku.edu.cn (Y. Cheng).

## 2. Experimental

Ti6Al4V scaffolds were fabricated using the EBM method based on a well-define "sliced" 3D CAD model. Ultrafine Ti6Al4V powders with particle sizes 45-100 µm were used. The cylindrical scaffold model (diameter 10 mm; height 5 mm) with a hexagonal periodic porous architecture was designed, as shown in Fig. 1B, and saved as 3D tomography data, which was imported by the software that controlled the EBM machine (Arcam AB. Sweden) and converted into 2D sliced data for EBM process. MAO was then carried out, with the EBM scaffold as anode, in 0.5 M NaOH solution by applying a pulsed AC field (500 Hz, 5%) at 320 V for 5 min using a IH-10 (Eco. Golden-Arc. Beijing) power supply. Musselinspired PD modification was in accordance with literature [13]. Briefly, the MAO samples were continuously shaken for 24 h in a solution of dopamine chloride (2 mg/ml, pH 8.5) at 37 °C. Next, PD modified samples (MAO/PD) were incubated in AgNO<sub>3</sub> (1 mM) for 6 h before being thoroughly rinsed and subjected to UV irradiation  $(\lambda = 254 \text{ nm}, 2.5 \text{ mW/cm}^2)$  for another 1 h to reduce silver. 100 scaffolds were as-produced and either material characterization or cell culture studies was done in triplicate (n=3).

Scanning electron microscopy (SEM, S4800, Hitachi, Ltd.) was employed to examine the surface morphology. The chemical composition and phase structure of the coatings were identified by energy-dispersive spectroscopy (EDS) and X-ray diffractometry (XRD, CuK $\alpha$  radiation,  $\lambda = 0.154$  nm), respectively. The in-vitro cytocompatibility were assessed using osteoblast-like MG63 cell lines. The subcultured cell passages were harvested and seeded onto the sterilized scaffolds at a density of  $1.5\times10^5$  cells/well, and incubated in a humidified atmosphere containing 5% CO $_2$  at 37 °C [14].  $\alpha\text{-}MEM$  supplemented with 10% FBS, 1% penicillin/streptomycin and 2 mM L-glutamine was used as culturing medium. Cells

cultured for 5 d were fixed with 2.5% glutaraldehyde and dehydrated in a series of ethanol. The cylinders were then cut into half to expose the interior architectures (Fig. 2B1), and coated with gold for SEM examination. Confocal laser scanning microscope (CLSM, Nikon ALR-SI) fluorescence images were recorded to visualize the distribution of cells on the engineered surfaces, by tomo-scanning and 3D reconstruction using the imaging software NIS-Elements AR 3.0. Briefly, the cells were fixed with 4% formaldehyde for 15 min, permeabilized with 0.1% Trion X-100 for 5 min, and stained with FITC-phalloidin (labeling actin filaments) for 40 min in the dark.

#### 3. Results and discussion

The EBM method allowed the production of highly porous cylinders with an open mesh structure. The 400  $\mu m$ -wide struts were fully-interconnected and formed hexagonal unit cells, visible in Fig. 1D. The cavity size and porosity were determined separately as  $(682\pm27)\,\mu m$  and  $(73.0\pm2.2)\,vol\%$ . These are important considerations since open continuous system with pores at optimal sizes facilitates mechanical interlocking and cell ingrowth, and consequently osteogenesis and bone remodeling [4].

After MAO/Ag treatment, the metallic surfaces became uniformly dark brown (Fig. 1E and F), a characteristic of oxidative polymerization of dopamine [13]. The macropores' walls of the EBM constructs had a  $\sim$ 1.8  $\mu$ m thick porous layer (outer-wall pores:  $\Phi$  0.5–2.5  $\mu$ m, inner-wall pores:  $\Phi$  0.1–1.0  $\mu$ m) with homogeneously immobilized AgNPs ( $\sim$ 50 nm; Fig. 2C–E). The layer is tightly-bonded without clear boundary or any crak, which is pivotal in load-bearing cases (Fig. 2B2). The MAO layer showed

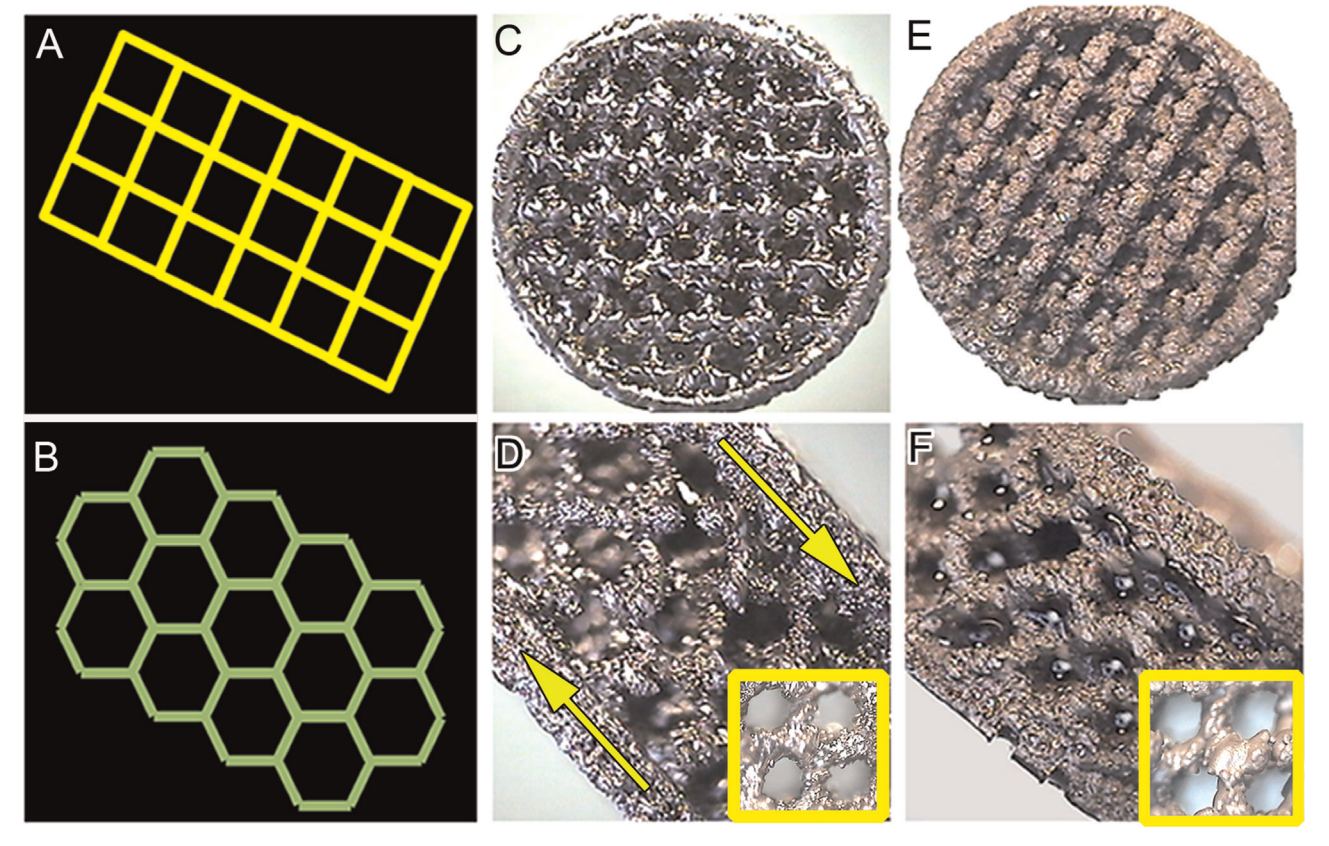


**Fig. 1.** The CAD model displaying the top (tetragonal, A) and oblique (hexagonal, B) cellular structure, and the EBM cylindrical scaffolds (D=10 mm, H=6 mm, strut width= $400 \mu \text{m}$ ) before (C, D) and after (E, F) MAO/Ag treatment. Insets in D and F are zoom-in pictures. Symmetrically-set rings (arrows in D) were designed to enhance mechanical strength.

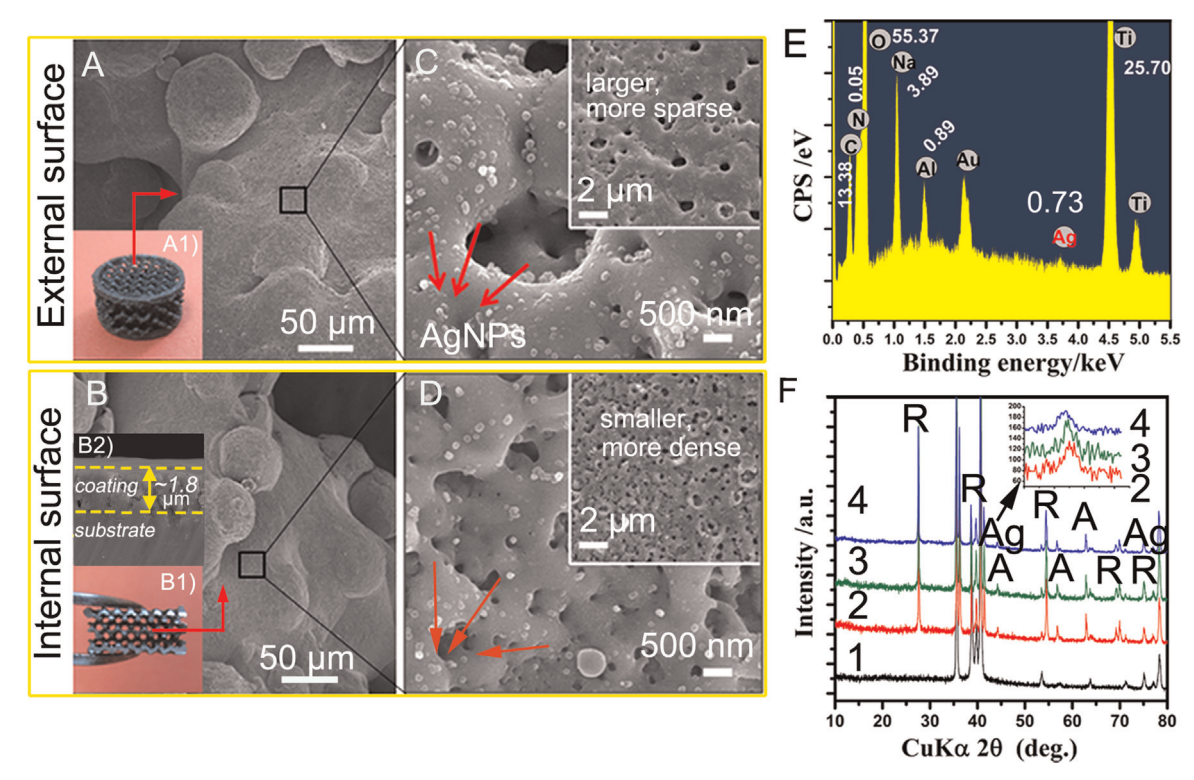
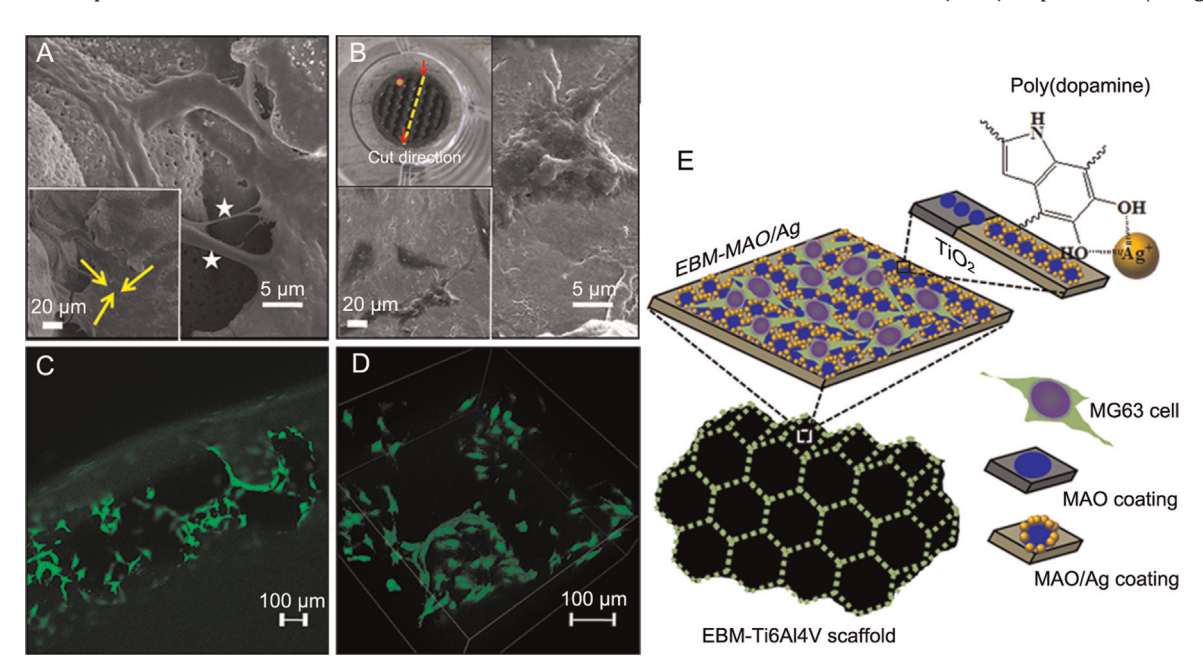


Fig. 2. External (A, C) and internal (B, D) surface morphology of the silver-immobilized multi-scaled porous Ti6Al4V alloy (insets A1, B1 are digital graphs, inset B2 is the cross section, insets in C, D are lower magnifications showing pore distribution); the  $\sim$ 1.8  $\mu$ m thick micro-nano porous titania layer was tightly-bonded to substrate (B2) and immobilized with homogeneous AgNPs, as verified by (E) and (F) (R = rutile, A = anatase). 1–4 in L represent the untreated, MAO, MAO/PD, and MAO/Ag treated alloys, respectively.

typical anatase and rutile phases based on the XRD patterns (Fig. 2F), while crystalline silver revealed additional diffraction peaks at  $2\theta$  values of  $44.4^{\circ}$  and  $77.5^{\circ}$ , which can be readily indexed to (200) and (310) facets of silver [15]. Note that the exterior and interior architectures were similarly coated, however, due to the geometrically-dependent discharging behavior [16], smaller and more dense micropores were observed within the scaffolds.

Surface adhesion and spreading of osteoblasts is a crucial indicator of implant bioactivity and long-term cellular behaviors (e.g. migration and differentiation) [17]. The MG63 cultured on the MAO/Ag scaffolds observed by SEM after 5 d of incubation (Fig. 3A) were well-adhered and displayed an elongated and wide-spread shape. Filopodia anchoring to the micropores and intercellular confluence, as well as extracellular matrix (ECM) sequestration/bridging were



**Fig. 3.** SEM images of MG63 morphology within the half-cut scaffolds (as indicated by top left inset in B) on day 5, (A) is the MAO/Ag treated and (B) the untreated one (bottom left insets are lower magnifications). Arrows and asterisks show confluence and bridging of cells, respectively. The CLSM projections of a representative area (the circle in top left inset in B) on the MAO/Ag treated scaffold are also obtained (C is an example); (D) is their 3D image stack, rendering the spatial cell extension. (E) Illustration of cell adhesion and spreading on the EBM-MAO/Ag surfaces.

observed. When it came to the untreated ones (Fig. 3B), the cells were sparsely distributed and less elongated with cytoplasmic extrusions, showing relatively little ECM and fewer filopodia. Further, the three-dimensional extension of MG63 on the engineered framework was confirmed by spatial cytoskeleton development. In our study, random areas were selected and they displayed highly analogical results, i.e., the cells spread and migrated continuously in a 3D manner, as exemplified by Fig. 3(C) and (D). It is expected that the pores would be gradually filled as proliferation proceeds.

These results indicated improved cytocompatibility verified from both morphology and cell quantity via the novel joint surface modification. The synergistic contribution of micro/nano-porous topography and adhesive chemical property of PD (increased surface hydrophilicity and bioactive functional groups (e.g. OH, NH<sub>2</sub>) [18]), as illustrated in Fig. 3E, could probably compensate adverse biological effects, if any, brought by AgNPs immobilization.

# 4. Conclusions

In conclusion, titanium scaffolds with hierarchical porosity were successfully developed via a combined EBM–MAO method. The micro-nanoporous MAO layer stimulated cell adhesion and considerably increased the cell number and improved cell morphology while subsequent nano-silver immobilization, inspired by the mussel's adhesive versatility, yielded potential antibacterial surfaces.

## Acknowledgments

This work was supported by Grants of the Project of Scientific and Technical Plan of Beijing (No. Z141100002814008), National Natural Science Foundation of China (No. 31370954), State Key

Laboratory of Bioelectronics Open Research Fund of China (Chien-Shiung Wu Laboratory), and National Basic Research Program (973) of China (2012CB619102). The authors would also acknowledge Beijing AKEC Medical Co. Ltd. for its efforts in EBM fabrication.

#### References

- [1] Y. Noyama, T. Miura, T. Ishimoto, T. Itaya, M. Niinomi, T. Nakano, Mater. Trans. 53 (2012) 565–570.
- [2] B.J.C. Luthringer, F. Ali, H. Akaichi, F. Feyerabend, T. Ebel, R. Willumeit, J. Mater. Sci.-Mater. Med. 24 (2013) 2337–2358.
- Sci.-Mater. Med. 24 (2013) 2337–2358.
  [3] S. Bose, S. Vahabzadeh, A. Bandyopadhyay, Mater. Today 16 (2013) 496–504.
- [4] E. Łyczkowska, P. Szymczyk, B. Dybała, E. Chlebus, Arch. Civ. Mech. Eng. 14 (4) (2014) 586–594.
- [5] L.H. Li, Y.M. Kong, H.W. Kim, Y.W. Kim, H.E. Kim, S.J. Heo, et al., Biomaterials 25 (2004) 2867–2875.
- [6] H.S. Ryu, W.H. Song, S.H. Hong, Surf. Coat. Technol. 202 (2008) 1853–1858.
- [7] Y.T. Sul, C. Johansson, E. Byon, T. Albrektsson, Biomaterials 26 (2005) 6720–6730.
- [8] R.O. Darouiche, N. Engl. J. Med. 350 (2004) 1422-1429.
- [9] Z. Li, D. Lee, X.X. Sheng, R.E. Cohen, M.F. Rubner, Langmuir 22 (2006) 9820–9823.
- [10] S.L. Mei, H.Y. Wang, W. Wang, L.P. Tong, H.B. Pan, C.S. Ruan, et al., Biomaterials 35 (2014) 4255–4265.
- [11] Y.H. Lee, F.Y. Cheng, H.W. Chiu, J.C. Tsai, C.Y. Fang, C.W. Chen, et al., Biomaterials 35 (2014) 4706–4715.
- [12] Y.L. Liu, K.L. Ai, L.H. Lu, Chem. Rev. 114 (2014) 5057-5115.
- [13] H. Lee, S.M. Dellatore, W.M. Miller, P.B. Messersmith, Science 318 (2007) 426–430.
- [14] M.A. Lopez-Heredia, J. Sohier, C. Gaillard, S. Quillard, M. Dorget, P. Layrolle, Biomaterials 29 (2008) 2608–2615.
- [15] T.H. Kim, M. Kim, H.S. Park, U.S. Shin, M.S. Gong, H.W.J. Kim, Biomed. Mater. Res. A 100A (2012) 1033–1043.
- [16] Y.Y. Yan, J.F. Sun, Y. Han, D.C. Li, K. Cui, Surf. Coat. Technol. 205 (2010) 1702–1713.
- [17] H. Ceylan, S. Kocabey, A.B. Tekinay, M.O. Guler, Soft Matter 8 (2012) 3929–3937.
- [18] C.T. Wu, P.P. Han, X.G. Liu, M.C. Xu, T. Tian, J. Chang, et al., Acta Biomater. 10 (2014) 428–438.